International Journal of Heat and Mass Transfer 52 (2009) 629–635

Contents lists available at ScienceDirect

International Journal of Heat and Mass Transfer

journal homepage: www.elsevier.com/locate/ijhmt

Multi-artery, heat pipe spreader

D.H. Min, G.S. Hwang, M. Kaviany *

Department of Mechanical Engineering, University of Michigan, 2250 G.G. Brown, Ann Arbor, MI 48109-2125, USA

ARTICLE INFO

Article history:
Received 20 March 2008
Received in revised form 11 July 2008
Available online 31 August 2008

Keywords:
Multiple liquid artery
Vapor chamber
Heat pipe
Optimal design
Dry out
Wick superheat

ABSTRACT

Multiple, columnar liquid vapor chamber allows for effective heat removal from finite, concentrated heat source by heat spreading via lateral vapor flow, while minimizing conduction resistance through thinner evaporator wick. The individual liquid arteries are designed by wick coated solid pillar. We optimize the artery geometry, numbers, and distribution, for both liquid and air-cooled, finned condensers, and show that the overall thermal resistance is substantially lower than the uniform wick vapor chamber.

1. Introduction

With smaller and faster microprocessors, heat removal from such concentrated sources pose challenges [1]. Using single-phase gas or liquid cooling, this concentrated heat should be spread over a sufficiently large area. Vapor chambers spread heat from concentrated sources to large condenser area, where it can be readily removed with high single-phase coolant streams. Vapor chamber (VC) is particularly effective in absence of any solid heat spreader added to the heat source (called internal heat spreader), where VC reduces the external coolant thermal resistance (due to the large area). The internal resistance of VC should be small enough such the overall thermal resistance R_Σ is small compared with no VC present.

The analysis of heat, vapor, and liquid flows in the asymmetric flat heat pipes are presented in [2] and a simplified conduction-based model for VC is given in [3], including the effect of gravity. The uniform wick VC [4] is easy to fabricate since it has a single, uniform liquid wick artery; however, it has a large conduction wick resistance. In [4] a centered, single wick column is placed above the heater area to circulate the liquid and ensure the structural stability VC. It decreases the distance of the liquid travels from condenser to evaporator, thus the evaporator wick thickness is reduced. However, it is also important to secure enough evaporation area to increase the heat flux through the wick. In [5] the measured and predicted heat flux in various modulated-wick heat pipes are presented and compared. One of models depicted as an artery–evaporator system with completely separated liquid and vapor flow paths, and this is similar to the multiple-artery heat pipe spreader proposed here.

We design a multiple artery VC to supply liquid for evaporation and reduce the evaporator wick thickness (where its conduction resistance is dominating). The geometric parameters such as artery diameter, numbers, and spacings, are optimized based on three-dimensional resistance network analyses for heat and fluid flows. We use external, air or water cooled, finned condenser and compare the overall thermal resistance with the uniform artery VC.

2. Multi-artery heat pipe spreader

The multi-artery heat pipe spreader (MAHPS) is a columnar vapor chamber heat pipe. An individual artery is designed by a solid pillar covered with a uniform wick as the liquid artery. This capillary artery draws the liquid from the condenser to the evaporator wick. Water is used as an operating fluid to achieve high capillary pressure (surface tension) and heat of vaporization. Fig. 1(a) and (b) shows the geometric parameters of MAHPS, and heat flow path from the heating source to the external, coolant. MAHPS is placed between the heater area and this external heat sink. The heat source is a constant heat flux condition and the coolant is far-field temperature and surface-convection resistance surface. Since the two temperatures for the T_h and T_c are predefined as constant, isothermal heat flux and constant coolant temperature boundary conditions, respectively, in this theoretical analysis, the saturation temperature depends on how much heat spreading occurs as the heater area. Phase change occurs at the liquid–vapor interface in the evaporator and condenser wicks [6]. During the phase change, the generated vapor moves toward the condenser, where it is uniformly condensed over a large area. Capillary pressure is used for

* Corresponding author. Tel.: +1 734 936 0402; fax: +1 734 615 6647.
E-mail address: kaviany@umich.edu (M. Kaviany).

0017-9310/$ - see front matter © 2008 Elsevier Ltd. All rights reserved.
doi:10.1016/j.ijheatmasstransfer.2008.07.021

Nomenclature

A	(cross-section) area (m^2)
c_p	specific heat (J/kg-K)
D	diameter (m)
d	(fin or column) diameter (m)
Δh_{lg}	enthalpy of vaporization (J/kg)
K	permeability (m^2)
k	thermal conductivity (W/m-K)
L	distance or height (m)
$\dot{M}$	mass flow rate (kg/s)
N	number
Nu_d	Nusselt number for coolant stream, crossflow over cylinder
p	pressure (Pa)
Pr	Prandtl number
Q	heat transfer rate (W)
R	resistance (K/W)
$\langle Re_d \rangle$	Reynolds number for coolant, crossflow over cylinder
r	radius (m)
T	temperature (K)
u	velocity (m/s)

Greek symbols

ϵ	porosity
η	efficiency
μ	viscosity (Pa-s)
ρ	density (kg/m^3)
σ	surface tension (N/m)

Subscripts

atm	atmosphere
b	bare area
c	capillary or column or condenser or coolant
c,c	center to center
e	evaporator
eff	effective
f	fin
g	vapor
h	heater
hex	hexagonal unit cell
i, j	node position
k	conduction
ku	surface-convection
l	liquid
lg	phase change or saturation
MA	multi-artery heat pipe spreader
max	maximum
min	minimum
p	particle
ps	pillar spacing
s	surface or solid
sh	superheat
Σ	overall (thermal resistance)
UA	uniform-artery heat pipe spreader
vc	vapor chamber
w	wick

the liquid circulation in MAHPS [7,8]. The critical geometric parameters of the baseline MAHPS are given in Table 1. For the baseline model, the heater diameter is 1 cm, and the condenser diameter is 5 cm. The wick covers the entire internal surface, including the evaporator wall and column walls, but different wick diameter, large sintered particles are used for the condenser and column, and small particles for the evaporator. In the baseline, the condenser-column and evaporator particle diameters are 200 and 50 μm, respectively. A hexagonal unit cell is used to calculate the axial and lateral heat flows, as well as the liquid pressure distribution. The thermophysical properties are evaluated at the saturation temperature of vapor which varies from 71.8 to 76.2 °C in the VC. The smaller the heater area, the lower the saturation temperature is (because of heat spreading). The effect of liquid convection in the thermal network is neglected (assuming small Péclet number [9]). In [6] the liquid and heat flow network models are designed for the steady-state analysis of the modulated wick heat pipe, and similar approach is used here.

3. Analysis using resistance thermal/hydraulics networks

3.1. Liquid flow resistance network

For the liquid flow network, the mass flow rates, $\dot{M}_{l,e}$ and $\dot{M}_{l,c}$ are calculated for each hexagonal unit cell (Fig. 1(a)). Assumptions for the network model are (i) liquid velocity is locally averaged, (ii) pressure drop by gravity is neglected, (iii) flow is Darcian and incompressible, (iv) liquid–vapor interface is in thermal equilibrium, (v) wick is isotropic, and (vi) condensation and evaporation occur on the wick surfaces [6]. Fig. 2(a) and (b) shows the thermal–hydraulic resistance network models. The liquid moves between the condenser wick and the evaporator wick. Evaporation on the evaporator wick surface is sustained by adjusting the capillary pressure by reducing the effective meniscus radius there. Since the condenser has the highest liquid pressure and we assume that in the outmost location on the condenser wick the capillary pressure is zero (i.e., $p_l = p_{lg}$). The radii difference between the evaporator and condenser gives the capillary pressure difference Young–Laplace equation [8]

$$\Delta p_c = \Delta p_l = \frac{2\sigma}{r_{c,e}} - \frac{2\sigma}{r_{c,c}}, \tag{1}$$

we have assumed uniform vapor pressure $p_g = p_{lg}$, where p_{lg} is the saturation pressure. σ is the surface tension, $r_{c,e}$ and $r_{c,c}$ are the meniscus radii at evaporator and condenser wick surfaces. We assume $r_{c,c}$ is infinity at the outmost corner of the condenser, and the maximum capillary pressure $p_{c,max}$ is [8]

$$p_{c,max} = p_g - p_{l,min} = \frac{2\sigma}{r_{c,min}} \cos\theta_c, r_{c,min} = (0.41)0.5 d_{p,e}, \tag{2}$$

where the θ_c is the contact angle and $d_{p,e}$ is the wick particle diameter for the evaporator wick. Here, $r_{c,min}$ is the minimum meniscus radius in Eq. (1) for sintered-particle wicks [10]. The material properties and relations are given in Table 2. Assuming that the liquid (l) and vapor (g) flow are incompressible (ii), the continuity equations are

$$\nabla \cdot u_l = 0 \quad \text{and} \quad \nabla \cdot u_g = 0, \tag{3}$$

where u_l and u_g are the liquid and vapor velocity vectors. The liquid mass flow rate is determined by heat flow from the constant, isothermal area, using the heat of evaporation Δh_{lg}

$$\dot{M}_l = \frac{Q}{\Delta h_{lg}} = \int_{A_{lg}} \dot{m}_{lg}\, dA, \tag{4}$$

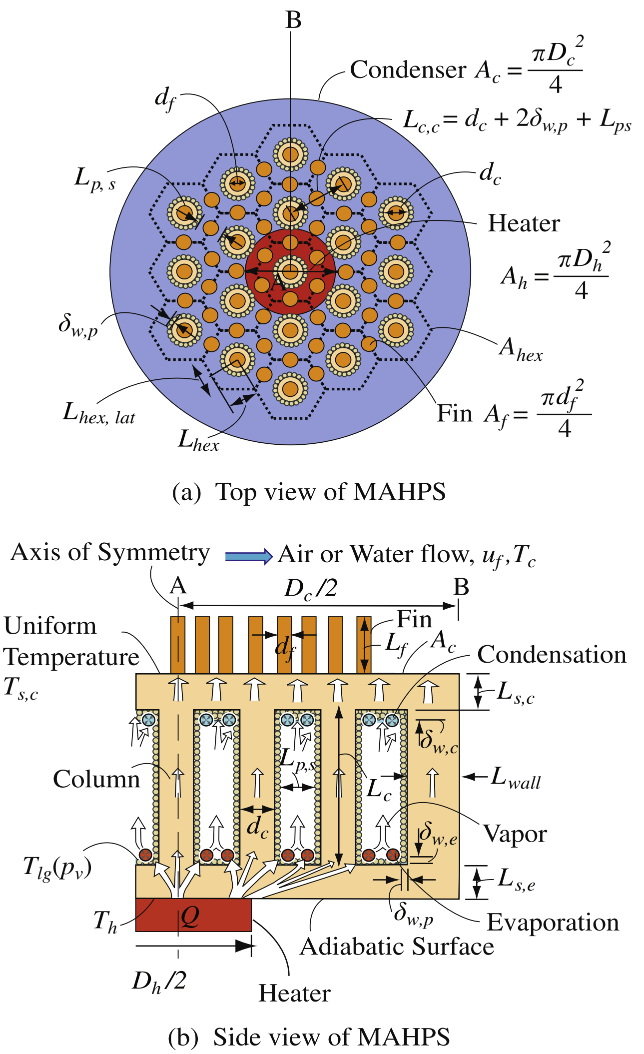

Fig. 1. Schematic of hexagonal unit cells around each column. (a) The size of each unit hexagonal cell varies with the column (pillar) diameter d_p, column wick thickness $\delta_{w,p}$, and column spacing $L_{c,c} = d_c + 2\delta_{w,p} + L_{p,s}$. The heater diameter D_h is also shown. (b) The cross-sectional area of MAHPS shows the heat flow paths as well as the geometric parameters.

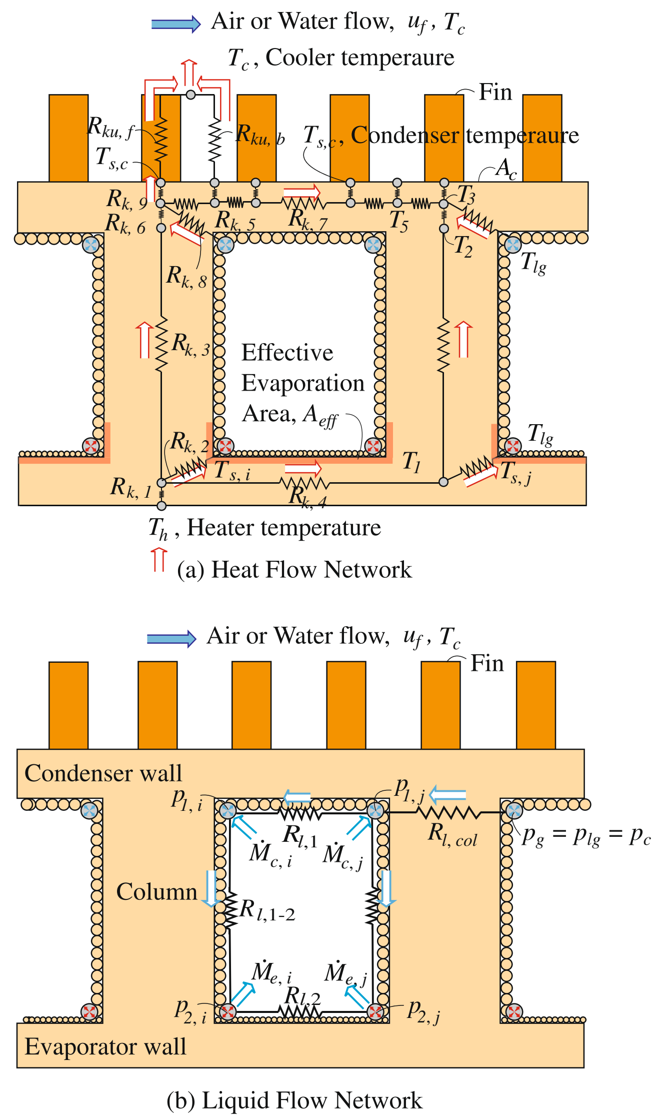

Fig. 2. Resistance network model for the thermal–hydraulic resistances assigned to each node per hexagonal unit cell. (a) The thermal resistances between adjacent temperature nodes. (b) In the wick structures, the hydraulic resistances are used between adjacent pressure nodes. The condensation and evaporation surfaces are also shown.

Table 1
Geometric parameters for the baseline MAHPS design

Geometric parameter	Magnitude
Heater diameter, D_h	1 cm
Condenser diameter, D_c	5 cm
Evaporator wall thickness, $L_{s,e}$	1 mm
Condenser wall thickness, $L_{s,c}$	1 mm
Side wall thickness, $L_{s,wall}$	1.5 mm
Evaporator wick particle diameter, $d_{p,e}$	50 µm
Condenser wick particle diameter, $d_{p,c}$	200 µm
(Uniform artery) wick particle diameter, d_p	100 µm
Evaporator wick thickness, $\delta_{w,e}$	50 µm
Condenser and column wick thickness, $\delta_{w,c}$	200 µm
(Uniform artery) wick thickness, δ_w	800 µm
Column diameter, d_c	1 mm
Column height, L_c	3 mm
Fin diameter, d_f	1 mm
Heat sink coolant number of fins (water), N_f	279

where $\dot{m}_{lg}$ is the local evaporation flux. Using the Darcy' law [11], the liquid pressure drop is

$$\Delta p_l = \frac{\mu_l L}{\rho_l K A}\dot{M}_l, \quad (5)$$

Table 2
Materials properties and relations used in heat and liquid flow network models (vapor chamber fluid: water)

Properties	Symbol	Magnitude/relations
Wick porosity	ϵ_e	0.3
	ϵ_c	0.4
Thermal conductivity	k_s	378 W/m-K
	k_w	0.66 W/m-K
	k_{air}	0.0287 W/m-K
	$\langle k_e \rangle$ (wick) [10]	$k_w\left(\frac{k_s}{k_w}\right)^{0.28-0.757\log_{10}\epsilon_e-0.057\log_{10}\frac{k_s}{k_w}}$
	$\langle k_c \rangle$	$k_w\left(\frac{k_s}{k_w}\right)^{0.28-0.757\log_{10}\epsilon_c-0.057\log_{10}\frac{k_s}{k_w}}$
Contact angle for water on copper	θ_c	0
Capillary pressure	p_c	$\frac{2\sigma}{(0.41)0.5d_{p,e}}$
Permeability	K_e [12]	$(0.41d_{p,e})^2\frac{4\epsilon_e^3}{180(1-\epsilon_e)^2}$
	K_c	$(0.41d_{p,c})^2\frac{\epsilon_c^3}{180(1-\epsilon_c)^2}$
Nusselt number for crossflow over cylinders	$\langle Nu \rangle_d$ [12]	5.37
Prandtl number	Pr	Water: 3.22, air: 0.69
Surface-convection resistance	$R_{ku,c}/A_c$	2×10^{-5} K/W-m^2

where μ_l is the liquid viscosity, L is the flow path length, $\dot{M}_l$ is the liquid mass flow rate, and ρ_l is the liquid density, K is the wick permeability determined from the Carman–Kozeny relation [12] listed in Table 2, and A is the cross-section area of the wick. Δp_l should be less than the maximum capillary pressure $p_{c,max}$ (i.e., $\Delta p_l \leqslant p_{c,max}$).

3.2. Heat flow resistance network

The assumptions for the heat flow resistance network are (i) local thermal equilibrium between solid and liquid in the wick, (ii) condensation occurs uniformly on the condenser surface, and (iii) vapor temperature (pressure) is uniform. The energy equation is

$$\nabla \cdot \boldsymbol{q} = 0, \tag{6}$$

under steady-state condition. The overall heat flow rate into the evaporator is

$$Q = \int_{A_e} (\boldsymbol{q} \cdot \boldsymbol{s}_n)\, dA = \dot{M}_{lg} \Delta h_{lg}, \tag{7}$$

where $\boldsymbol{s}_n$ is the surface normal unit vector and A_e is the evaporation area. Due to low liquid velocity in MAHPS leads to the low Péclet numbers, only conduction is considered in heat flow network. For the heat flow network, the thermal conduction resistance R_k based on one-dimensional heat conduction is

$$Q_k = \frac{\Delta T}{R_k}, \quad R_k = \frac{L}{kA_k}, \tag{8}$$

where k is the thermal conductivity, A_k is the cross-section area, ΔT is temperature between the nodes i and j, shown in Fig. 2(a). The wick superheat ΔT_{sh} is

$$\Delta T_{sh} = T_{s,i} - T_{lg}. \tag{9}$$

where $T_{s,i}$ is the average temperature under the evaporator wick (Fig. 2(a)). The temperature on the wick surface is the saturation temperature T_{lg} and is assumed uniform within MAHPS.

3.3. Resistances

The liquid pressure drop in the condenser wick and the corresponding liquid resistance are

$$\Delta p_1 = \frac{\mu_l L_{p,s}}{\rho_l K_c A} \dot{M}_{l,c} = R_{l,1} \dot{M}_{l,c}, \tag{10}$$

where the cross-section area $A = L_{hex,lat}\delta_{w,c}$ and $\dot{M}_{l,c}$ is the condensation rate. The arrows shown in Fig. 2(b) indicate the direction of liquid flow. The pressure drop along the column wick is

$$\Delta p_{1-2} = \frac{\mu_l L_c}{\rho_l K_c A}\left(\dot{M}_{l,c} - \dot{M}_{l,e}\right) = R_{l,1-2}\left(\dot{M}_{l,c} - \dot{M}_{l,e}\right), \tag{11}$$

where the cross-section area $A = \pi[((d_c + 2\delta_{w,e})^2 - d_c^2)]/4$, $\dot{M}_{l,e}$ is the liquid evaporation rate in the evaporator wick. The evaporator pressure drop is

$$\Delta p_2 = 0.25 \frac{\mu_l L_{p,s}}{\rho_l K_e A} \dot{M}_{l,c} = R_{l,2} \dot{M}_{l,c}, \tag{12}$$

where the cross-section area $A = \pi[(d_c + 2\delta_{w,c})\delta_{w,e}]/2$ and the evaporation is assumed to occur over 1/4 of $L_{p,s}$. This is a simplifying assumption noting the liquid spreads short distance over the evaporator. More elaborate model may allow for local evaporation over a network preceding this region, but is not pursued here. The liquid resistance $R_{l,col}$ shown in Fig. 2(b) across column is given as

$$R_{l,col} = 0.5 \frac{\mu_l (R_c - N_r L_{hex})}{\rho_l K_c A}, \tag{13}$$

where the N_r is the number of rings of hexagonal unit cell, and the liquid path is determined from N_r. Here, A is the cross-section area of the inter-column defined as $A = \pi(D_e + N_r L_{hex})\delta_{w,c}$. The liquid flow rate for each hexagonal unit cell is

$$\dot{M}_{l,i} = \frac{Q}{N_{hex} \Delta h_{lg}}, \tag{14}$$

where Q is the heat flow rate defined by the heat flow rate across the wick and N_{hex} is the number of hexagonal unit cells.

For the heat flow network, the entire geometry (evaporator and condenser wall, column, wick structure, and finned condenser) is included in the network. The axial and lateral heat flow resistances of VC are given as

$$R_k = \frac{L}{kA}, \tag{15}$$

where L is the distance for heat flow, k is thermal conductivity, and A is the cross-section area normal to the heat flow. Since heat flows toward to the evaporator wall and the column, the resistance across the evaporator wick is defined by an effective evaporation area. As shown in Fig. 2(a), the effective evaporation area is

$$A_{eff} = 0.5\pi d_c L_{p,s} + \left[A_{hex} - \pi(d_c + 2\delta_{w,e})^2\right]. \tag{16}$$

The heat flow resistance of the finned external coolant is given next.

3.4. Heat sink (external coolant stream)

Fig. 1(b) shows the finned condenser top of VC. Since the surface-convection of air is less effective than water as coolant, the surface area should be increase (from the baseline which is for water). The geometric parameters are the number of fins, the diameter and the length of the fin, and the area of the condenser. The surface-convection resistance is

$$\frac{1}{R_{ku,c}} \equiv A_b Nu_d \frac{k_f}{d_f} + \eta_f A_f Nu_d \frac{k_f}{d_f}. \tag{17}$$

The Nu_d is given by the correlation for crossflow over cylinders [13]. The fin surface area A_f and flat area A_c and the bare area A_b, are

$$A_f = N_f\left(\pi d_f L_f + \frac{\pi d_f^2}{4}\right), \quad A_c = \frac{\pi D_c^2}{4}, \quad A_b = A_c - N_f\left(\frac{\pi d_f^2}{4}\right). \tag{18}$$

The same heat flow rate through MAHPS is removed through the finned condenser, i.e.,

$$Q = \frac{T_h - T_c}{R_\Sigma}, \tag{19}$$

where the overall resistance, R_Σ is given in Table 4. Here, we use $\eta_f = 1$ (i.e., relatively short fins).

4. Result and discussion

We now proceed to minimize R_Σ for MAHPS, and make comparison with the single, uniform artery performance.

4.1. Effect of internal column geometry

Fig. 3 shows the variation, as a function of artery diameter d_c, for $L_{c,c} = 3.0$ mm, and D_h = 1 cm. As the diameter is reduced, R_Σ decreases. Although the thermal conductivity of the solid portion of the column (copper) is higher than the wick (sintered copper particle), the dominant heat transfer occurred is towards the evaporation surface. Increase in d_c also reduce the evaporation area. So MAHPS performance improves when the evaporation area is increased by reducing d_c. However, there is a minimum column

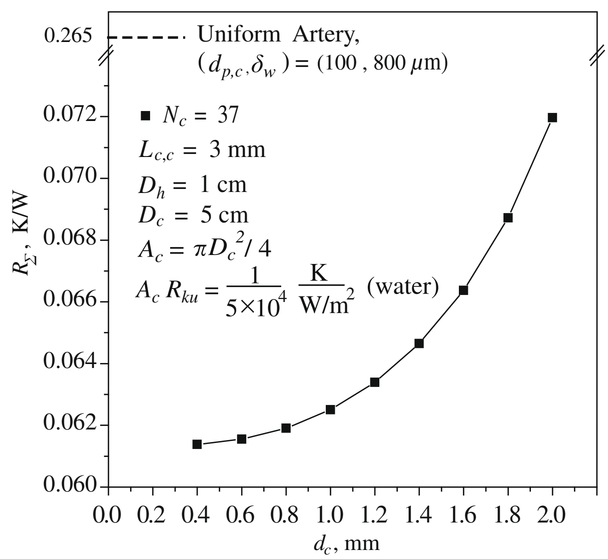

Fig. 3. The overall thermal resistance for MAHPS, as a function of column diameter. The overall thermal resistance for the uniform artery is also shown.

diameter, to avoid liquid chocking through the columns. The pressure drop is limited by the maximum capillary pressure, and this occurs when the column diameter is less than 0.4 mm. In addition, the conduction resistance through the column sharply increases and R_Σ increases, for $d_c \leqslant 0.4$ mm. As shown in Fig. 3, the thermal resistance is inversely proportional to the evaporation area until the liquid pressure drop reaching the maximum capillary pressure. The uniform, single artery has no columns, so it has more evaporation area compared to MAHPS. However, its overall thermal resistance is about four times higher than MAPHS, due to its thick wick to avoid liquid chocking limit. Since the liquid path from condenser to evaporator in the uniform artery is longer than MAHPS, its liquid pressure drop along the wick is higher than MAHPS. Thus, the evaporator wick thickness should increase to avoid dryout and the wick conduction resistance increases. These comparisons are also listed in Table 3.

4.2. Effect of heater size

Fig. 4 shows the variation of overall thermal resistance with respect to the heater diameter. Here, a simplified model is used to predict maximum and minimum bounds of R_Σ, where one-dimensional heat flow (no heat spreading in the evaporator wall and wick, and no area reduction due to presence of columns) is assumed. The simplified model is

Table 3
Overall thermal resistance R_Σ for various internal column diameter ($L_{c,c}$ = 3.0 mm)

MAHPS	d_c (mm)	R_Σ (K/W)
$L_{c,c} = 3$ mm	0.4	0.0614
$N_c = 37$	0.6	0.0616
$\delta_{w,p} = 200$ μm	0.8	0.0619
$\delta_{w,c} = \delta_{p,c} = 200$ μm	1.0	0.0625
$\delta_{w,e} = \delta_{p,e} = 50$ μm	1.2	0.0634
	1.4	0.0646
	1.6	0.0664
	1.8	0.0687
	2.0	0.0720
Uniform artery	δ_w (mm)	
$L_{c,c} = 3$ mm	0.8	0.265

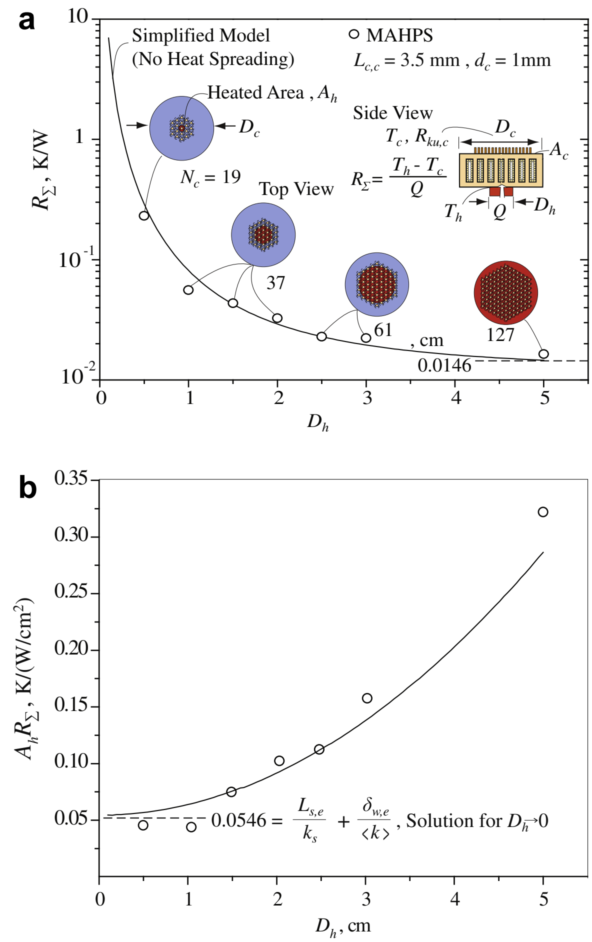

Fig. 4. (a) Comparison overall thermal resistance of MAHPS (axial and radial network model) with the simplified model (based on the one-dimensional network), a function of heater diameter. The number of columns indicates the heat spreading in the radial direction. (b) Same for the thermal resistance multiplied by the heater area. The asymptotic thermal resistance for small heater area is also shown.

$$R_\Sigma = \frac{1}{A_h}\left(\frac{L_{s,e}}{k_s} + \frac{\delta_{w,e}}{\langle k_e \rangle}\right) + \frac{1}{A_c}\left(\frac{L_c}{k_v} + \frac{\delta_{w,c}}{\langle k_c \rangle} + \frac{L_{s,c}}{k_s} + \frac{A_c}{R_{ku,c}}\right), \quad (20)$$

where A_h is heater area where the constant, isothermal heat flux boundary condition is applied, $L_{s,e}$ is evaporator wall thickness, $\delta_{w,e}$ and $\delta_{w,c}$ are evaporator and condenser wick thicknesses, A_c is surface area of condenser, L_c is the distance between evaporator area and condenser wick, and $R_{ku,c}$ is the surface-convection resistance of coolant stream. k_v of 10^5 W/m-K is used since the thermal resistance of evaporated vapor is negligibly small [3]. From Eq. (20), the minimum of R_Σ is 0.0146 K/W, when the heater has the same size of the condenser. R_Σ is larger than this lower limit for MAHPS, shown in Fig. 4. The top view shows the number of columns when the total Q is maximized. For small D_h, the area covered by columns is relatively larger than the heater area, which implies heat spreading. As the aspect ratio of the heater and evaporator, or the thickness of the evaporator wall, is increased, more spreading occurs in the evaporation area and R_Σ increases due to this heat spreading [1]. For D_h < 1.5 cm diameter, MAHPS R_Σ is less than the simplified model. This implies that the bottleneck for reducing the overall thermal resistance is the thermal resistance through the evaporator wall and wick. However, for D_h > 1.5 cm, heat spreading near the heater does not contribute to the thermal resistance. It indicates that the external coolant resistance play a large role in R_Σ. Fig. 5 shows the amount of heat transferred through MAHPS, as a function

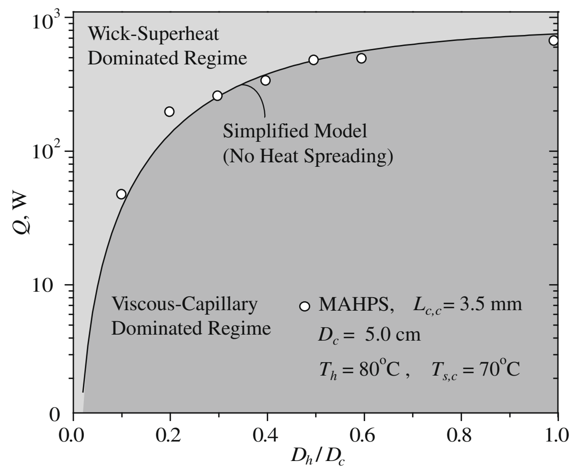

Fig. 5. Critical heat flow rate (dry-out limit) as a function of dimensionless heater diameter.

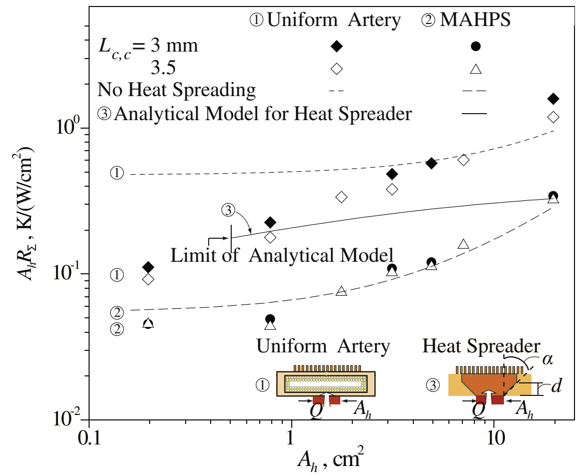

Fig. 6. Comparison of the overall thermal resistance of MAHPS, the uniform artery design, and the solid copper spreader, as a function of heater area. The parameters in the solid copper spreader and the uniform artery design are also shown.

of D_h/D_c. The wick-superheat dominated regime and viscous-capillary dominated regime are marked. A maximum evaporator wick superheat of 10 °C is assumed from the pool boiling experiments [14]. The viscous-capillary limit is smaller than the superheat limit. Values of R_Σ as a function of heater diameter, are also listed in Table 4.

4.3. Comparison with solid copper heat spreader and uniform wick

The columns in MAHPS reduce the overall flow resistance, since the condensate directly moves to the heater area. For the uniform artery, the liquid flow path is longer, this increases the overall liquid flow resistance, while its evaporation area is larger than MAHPS. Fig. 6 shows variation of R_Σ for uniform artery, MAHPS, and a solid copper heat spreader [15], as a function of A_h. For the uniform artery, the wick thickness is 800 μm and for MAHPS, the evaporator wick thickness is 50 μm, and this results in larger R_Σ for the uniform artery. However, there is only a small difference between the two for small A_h. Although the conduction resistance of MAHPS is less than the uniform artery, the effect of heat spreading compensates. For small heater diameter, the area for evaporation is critical. If the heater diameter is equal or smaller than the MAHPS column diameter d_c, there is no reduction in $A_h R_\Sigma$ [4].

Although the vapor spreads heat uniformly, thus reducing the overall thermal resistance substantially, MAHPS may potentially be disadvantageous, compared with a solid copper heat spreader due to its low wick effective thermal conductivity. Using the analytical model for R_Σ in solid copper heat spreader [15], the results for MAHPS, uniform artery, and the solid copper heat spreader, are compared in Fig. 6. The overall (no interfacial material or resistance) R_Σ for the solid copper heat spreader is [15]

$$R_\Sigma = \int_0^d \frac{\cos\alpha^{-1}}{(D_h/2 + \tan\alpha x)^2 \pi k_s}\,dx + \frac{A_c}{(D_h/2 + \tan\alpha d)^2 \pi R_{ku,c}}, \qquad (21)$$

where $\alpha = 70°$ is used as a spreading angle in the solid copper heat spreader and d is the total spreading thickness. The material properties are those listed in Table 2. Fig. 6 shows that $A_h R_\Sigma$ for the solid copper heat spreader is lower than the uniform artery, but higher than MAHPS. Since the heat spreadability of the vapor reduces $A_h R_\Sigma$ substantially, MAHPS shows better performance compared to the solid copper heat spreader. In Fig. 6, the simplified model for the uniform artery (no heat spreading) is differ, from the results of its network model. This is because heat spreading occurs inside the thick wick which reduces $A_h R_\Sigma$ in network model as A_h decreases. Thus, for small A_h there is a small difference between the uniform artery and the solid heat spreader.

In Fig. 6, $A_h R_\Sigma$ depends on the column spacing $L_{c,c}$. This implies that the size of hexagonal unit cell given by $L_{c,c}$, influences the accuracy of the network model results, the placement of the columns in the heater area is determined (constrained) by this unit-cell size. However, this is not a large difference in $A_h R_\Sigma$. The numerical values used in Fig. 6 are also given in Table 5.

4.4. Effect of coolant

For an air cooled condenser, the number of fins and condenser diameters are found for the same cooling performance as water as the coolant ($R_{ku,c}$). The results are shown in Fig. 7, and compare with those of water cooled condenser (baseline design). Although air cooled condenser requires a larger surface area and number of fins, the results show a moderate condenser diameter and number of fins of the air-cooled heat sink.

Table 4
Overall thermal resistance R_Σ for the various heater diameter ($L_{c,c}$ = 3.5 mm)

N_c	D_h/D_c	D_h (cm)	$A_h R_\Sigma$ (K/(W/cm²))	Q (W)	ΔT_{sh} (°C)
19	0.1	0.5	0.0454	43.2	4.01
37	0.2	1.0	0.0438	179	3.50
	0.3	1.5	0.0749	236	3.22
	0.4	2.0	0.102	307	3.02
61	0.5	2.5	0.112	436	2.35
	0.6	3.0	0.158	449	2.25
127	1.0	5.0	0.322	610	1.13

Table 5
Comparison of overall thermal resistance R_Σ between MAHPS (MA) and uniform artery (UA) design

A_h (cm²)	N_c	$L_{c,c}$ = 3 mm				$L_{c,c}$ = 3.5 mm			
		$A_h R_{\Sigma,MA}$	Q_{MA}	$A_h R_{\Sigma,UA}$	Q_{UA}	$A_h R_{\Sigma,MA}$	Q_{MA}	$A_h R_{\Sigma,UA}$	Q_{UA}
0.196	19	0.0454	43.3	0.111	17.7	0.0454	43.2	0.0919	20.1
0.785	37	0.0491	160	0.223	34.8	0.0438	179	0.178	22.5
1.77		–	–	–	–	0.0749	236	0.336	48.1
3.14		0.109	289	0.483	65.0	0.102	307	0.380	75.2
4.91	61	0.120	409	0.573	85.7	0.112	436	–	–
7.07		–	–	–	–	0.158	449	0.605	104
19.6	127	0.342	574	1.58	124	0.322	610	1.19	152

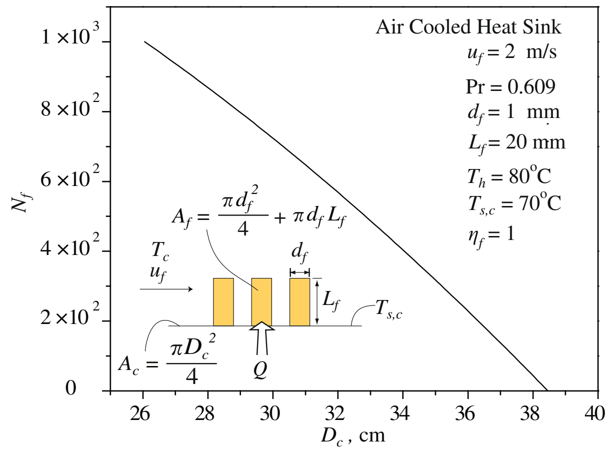

Fig. 7. Variation of predicted minimum number of fins for air cooled condenser, with respect to condenser diameter. The fin geometry is also shown.

5. Conclusions

In this paper, the network model for MAHPS is developed to optimize its three-dimensional heat and liquid flow. The baseline design uses water as external coolant, and air cooling is also considered. The results show while large number of columns is needed to make the most of the maximum capillary pressure by removing the most heat, the columns also limit the evaporation area. For a 1 cm diameter heater in a 5 cm diameter VC, the optimized number of columns is about 37. In addition to the viscous-capillary limit, we also use the evaporator wick-superheat limit set at 10 °C. MAHPS shows superior performance compared to the uniform artery, by reducing its overall thermal resistance.

Acknowledgements

We are thankful for useful discussions with Dr. Christian Terp of Asetek A/S (Denmark).

References

[1] S. Lee, Calculating spreading resistance in heat sinks, Electron. Cool. 4 (1998) 30–33.
[2] K. Vafai, W. Wang, Analysis of flow and heat transfer characteristics of an asymmetrical flat plate heat pipe, Int. J. Heat Mass Transfer 35 (1992) 2087–2099.
[3] R.S. Prasher, A simplified conduction based modeling scheme for design sensitivity study of thermal solution utilizing heat pipe and vapor chamber technology, J. Electron. Packaging 125 (2003) 378–385.
[4] S.S. Hsieh, R.Y. Lee, J.C. Shyu, S.W. Chen, Analytical solution of thermal resistance of vapor chamber heat sink with and without pillar, Energy Convers. Manage. 48 (2007) 2708–2717.
[5] S.G. Liter, M. Kaviany, Pool-boiling CHF enhancement by modulated porous-layer coating: theory and experiment, Int. J. Heat Mass Transfer 44 (2001) 4287–4311.
[6] G.S. Hwang, M. Kaviany, W.G. Anderson, J. Zuo, Modulated wick heat pipe, Int. J. Heat Mass Transfer 50 (2007) 1420–1434.
[7] S.D. Garner, J.E. Toth, Heat pipes: a practical and cost effective method for maximizing heat sink effectiveness, in: Proceedings of Pacific Rim/ASME International Intersociety Electronic and Photonic Packaging Conference (InterPACK), Kohala Coast, June15–19, 1997, vol. 2, pp. 1897–1902.
[8] G.P. Peterson, An Introduction to Heat Pipes: Modeling, Testing, and Applications, Wiley, New York, 1994.
[9] Z.J. Zuo, A. Faghri, A network thermodynamic analysis of the heat pipe, Int. J. Heat Mass Transfer 41 (1997) 1473–1484.
[10] S.W. Chi, Heat Pipe Theory and Practice, McGraw-Hill, New York, 1976.
[11] D.A. Reay, Advances in heat pipe technology, in: Proceedings of the IVth International Heat Pipe Conference 7–10 September 1981, Pergamon, London, UK, 1981.
[12] M. Kaviany, Principles of Heat Transfer in Porous Media, second ed., Springer, New York, 1995.
[13] M. Kaviany, Principles of Heat Transfer, Wiley, New York, 2001.
[14] G.S. Hwang, M. Kaviany, Critical heat flux in thin, uniform particle coatings, Int. J. Heat Mass Transfer 49 (2006) 844–849.
[15] C.N. Rasmussen, C.B. Terp, Optimal design of coldplates for cpu coolers, HT2007-32376, 2007 ASME-JSME Thermal Engineering Summer Heat Transfer Conference, Vancouver, British Columbia, Canada, 2007.